

A FACETED SHAPE MODEL APPROACH TO ALTIMETRY AND VELOCIMETRY FOR IRREGULARLY SHAPED BODIES

D.S. Bayard, P.B. Brugarolas and S.B. Broschart

Jet Propulsion Laboratory
California Institute of Technology
4800 Oak Grove Drive
Pasadena, CA 91109

ABSTRACT

Range and velocity sensors based on lidar or radar with multiple beams are often used to measure the altitude and velocity, respectively, of a spacecraft above a target body. A difficulty that arises when navigating about small bodies such as asteroids or comets, is that the notion of altitude is largely obscured by the irregular shape of the target surface. This paper develops a method to incorporate the multibeam altimeter and Doppler velocimeter measurements into the on-board spacecraft state estimator by using information from a faceted shape model representation of the target body surface. The faceted shape model representation is very general and does not place any restriction on the surface complexity. This allows the estimation method to be applicable to a broad class of irregularly shaped target bodies.

1 INTRODUCTION

Spacecraft exploration over the last decade has been expanding in many new directions. One important direction is the exploration of small bodies such as asteroids and comets. Recent missions include the Deep Space 1 mission that flew-by the comet Borrelly [5], the Near Earth Asteroid Rendezvous (NEAR) mission that orbited and eventually landed on the asteroid Eros [13], the 2004 Stardust mission that flew through the tail of comet Wild 2 [4], and the Deep Impact mission that drove an impactor at high velocity into comet Temple 1 [11]. Challenging on-going missions include the Japanese Hayabusa mission (formerly MUSES-C) launched in 2003 that touched down two times on asteroid Itokawa and is bringing a sample back to Earth [12], and the European Rosetta mission [10] launched in 2004 and scheduled to orbit and land on comet 67P/Churyumov-Gerasimenko in 2014.

Altimeters and velocimeters are important sensors for supporting navigation about small bodies. A difficulty that often arises when trying to use altimeters or velocimeters for small body navigation is that the notion of altitude is obscured by the irregular shape of the body

(cf., Figure 1.1). This report overcomes this difficulty by making use of a faceted shape model, possibly high-order, to represent the intricate shape of the target body. The use of faceted shape models to represent complex 3-dimensional objects is very common in the computer graphics community and has become a dominant paradigm in the movie and video game industries. Likewise, facet models are a natural choice for supporting an on-board state estimator that requires an accurate internal representation of the target body's shape. An approach is developed in this paper to systematically incorporate the multibeam altimeter and/or velocimeter measurement into the state estimator by making use of information from a faceted shape model. The approach makes use of Hesse's normal form to represent the shape model's planar facets. This particular representation is motivated by an approach taken in an earlier study [6]. The data structure developed is called the Range Measurement Table (RMT) for the altimeter measurement, and the Velocity Measurement Table (VMT) for the velocimeter measurement. The resulting measurement updates based on the RMT and VMT data types lead to spacecraft estimation solutions for very general classes of irregularly-shaped target bodies. All results in this paper have been taken from a series of JPL reports [1][3][6].

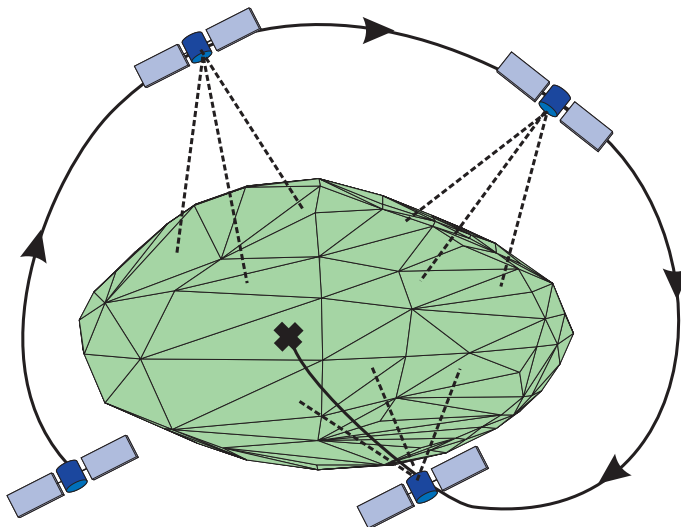


Figure 1.1: Spacecraft navigation about a small body is aided by altimetry and velocimetry measurements taken relative to an irregularly-shaped target body.

2 BACKGROUND

2.1 Frames and Vectors

The main frames and vectors in the small body problem are depicted in Figure 2.1. For simplicity, only one altimeter beam and one facet are shown. However, treatment will be generalized later to multiple beams and multiple facets.

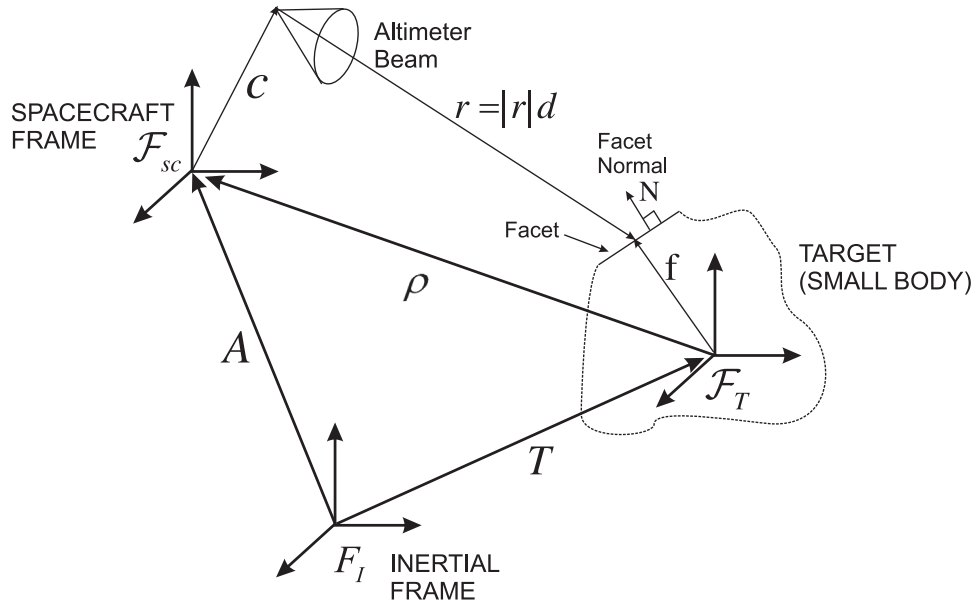


Figure 2.1: Frames and vectors used in the small body problem.

Let all vectors with under-arrows (e.g., \underline{x}), be coordinate free. The beam index i will be dropped for the time being, and we will consider a generic beam. Consistent with Figure 2.1, it will be convenient to define the following frames and coordinate free quantities associated with a generic beam intersecting a generic facet of the small body model.

\mathcal{F}_I - Inertial Frame, located at Solar System CM (center-of-mass)

\mathcal{F}_T - Target Body Frame, located at Target Body CM

\mathcal{F}_{sc} - Spacecraft Body Frame, located at S/C CM

\underline{r} - Position vector from beam origin on Spacecraft to beam intersection point on Target Body facet (coordinate-free)

\underline{f} - Position vector from Target Body CM to beam intersection point on Target Body facet (coordinate-free)

\underline{c} - Position vector from Spacecraft CM to beam origin (coordinate-free)

\underline{d} - Unit vector direction of beam (coordinate-free)

\underline{N} - Unit normal vector associated with Target Body facet that the beam intersects (coordinate-free)

2.2 Facet Plane Geometry

The geometry of a facet plane is shown in Figure 2.2. Consider any two vectors $\underline{\ell}_1$ and $\underline{\ell}_2$ that start at the Target Body CM and have their heads lying on the facet plane. Then one can write,

$$\underline{\epsilon} = \underline{\ell}_2 - \underline{\ell}_1 \quad (2.1)$$

where the vector $\underline{\epsilon}$ lies in the facet plane. Accordingly, $\underline{\epsilon}$ must be perpendicular to the facet normal \underline{N} ,

$$\underline{N} \cdot \underline{\epsilon} = 0 \quad (2.2)$$

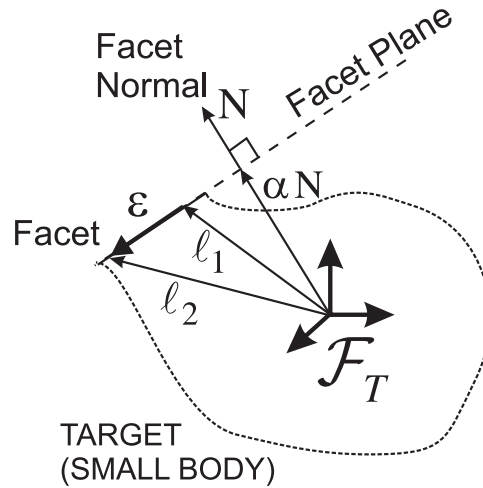


Figure 2.2: Geometry of a facet plane.

Substituting (2.1) into (2.2) and rearranging yields,

$$\underline{N} \cdot \underline{\ell}_2 = \underline{N} \cdot \underline{\ell}_1 \quad (2.3)$$

We can conclude that the inner product of the facet normal \underline{N} with any vector $\underline{\ell}$ starting at the Target Body CM and having its head on the facet plane gives the same constant value. This constant is important and will be denoted as the *facet constant* κ . Each facet will have its own value of κ . For a given facet,

$$\underline{N} \cdot \underline{\ell} = \kappa \quad (2.4)$$

where $\underline{\ell}$ is any vector starting at the Target Body CM and having its head on the facet plane. Choosing $\underline{\ell} = \alpha \underline{N}$ (i.e., the vector perpendicular to the facet plane with length α), in (2.4) gives,

$$\kappa = \alpha(\underline{N} \cdot \underline{N}) = \alpha \quad (2.5)$$

Hence κ can be interpreted physically as the perpendicular distance (i.e., the minimal distance), from the Target Body CM to the facet plane. The use of relation (2.4) in the current report is motivated by the treatment given in [6], and will be important for later derivations.

REMARK 2.1 If values for \underline{N} and κ are specified, equation (2.4) can be used as a *definition* of the facet plane. This particular definition of a plane is known in tensor analysis as *Hesse's normal form* [15].

3 RANGE MEASUREMENT TABLE (RMT)

The Range Measurement Table (RMT) is a table of measured ranges along known beam directions. The format of the RMT is shown in Table 3.1, where each row of the RMT corresponds to a range measurement along a different beam direction. There are m rows corresponding to at most m possible beams. While the actual number of beams is not limited, 3 or 4 beams are typical. The first column is the row index, and the second column is a number from 0 to 1 representing the confidence in the measurement. For the present, these confidences are taken as either 0 or 1, indicating a complete rejection or acceptance of the measurement, respectively. The quantity y corresponds to the scalar range measurement from the i 'th beam, and σ is its associated 1-sigma error value. Currently, noises on each beam are assumed to be statistically independent. The quantity \mathbf{N} is the unit normal of the facet associated with the i 'th beam's intercept point on the Target Body surface, and κ is its associated facet constant. Typically, the intersection point of the altimeter beam with the shape model is not known exactly, and must be estimated based on the current state estimate. A procedure for doing this is given in [7]. The quantity d represents the unit vector direction of the i 'th beam, and c represents the offset vector from the spacecraft CM to the i 'th beam origin.

#	Conf	$y =$ $ r $	σ	$\mathbf{N}^T =$ $[N_x, N_y, N_z]$	κ	$\mathbf{d}^T =$ $[d_x, d_y, d_z]$	$\mathbf{c}^T =$ $[c_x, c_y, c_z]$
1							
2							
\vdots							

Table 3.1: Range Measurement Table (RMT) specifying range along known beam directions

From the geometry shown in Figure 2.1,

$$\underline{f} = \underline{\rho} + \underline{c} + \underline{r} \quad (3.1)$$

Since the head of vector f lies on the facet plane, it satisfies Hesse's normal form (2.4),

$$\underline{N} \cdot \underline{f} = \kappa \quad (3.2)$$

Substituting (3.1) into (3.2) gives,

$$\underline{N} \cdot (\underline{\rho} + \underline{c} + r) = \kappa \quad (3.3)$$

This implies,

$$\underline{N} \cdot (\underline{\rho} + \underline{c} + |r|\underline{d}) = \kappa \quad (3.4)$$

or equivalently,

$$|r|(\underline{N} \cdot \underline{d}) = \kappa - \underline{N} \cdot \underline{\rho} - \underline{N} \cdot \underline{c} \quad (3.5)$$

where $\underline{r} = |r|\underline{d}$. Solving for the range $|r|$ in (3.5) gives,

$$|r| = \frac{\kappa - \underline{N} \cdot \underline{\rho} - \underline{N} \cdot \underline{c}}{\underline{N} \cdot \underline{d}} \quad (3.6)$$

The condition $\underline{N} \cdot \underline{d} = 0$ is not expected to occur in practice since it corresponds to the beam direction being perpendicular to the facet normal. This condition can be tested in-flight before applying the measurement update.

Now the variables c_i, d_i, f_i, r_i, N_i are specialized to be associated with the i 'th beam and the following choices are made for their coordinate frames,

$$f_i, N_i \in \text{Target Body frame } \mathcal{F}_T \quad (3.7)$$

$$r_i, c_i, d_i \in \text{S/C body frame } \mathcal{F}_{sc} \quad (3.8)$$

$$\rho \in \text{Inertial frame } \mathcal{F}_I \quad (3.9)$$

κ_i - Scalar facet constant associated with Target Body facet that i 'th beam intersects

r_i - Position vector from i 'th beam origin to its intersection point on Target Body facet, resolved in Inertial \mathcal{F}_I

f_i - Position vector from Target Body CM to i 'th beam intersection point on Target Body, resolved in \mathcal{F}_T

c_i - Position vector from Spacecraft CM to i 'th beam origin, resolved in \mathcal{F}_{sc}

d_i - Unit vector direction of i 'th beam, resolved in \mathcal{F}_{sc}

N_i - Unit normal direction vector of facet that i 'th beam intersects, resolved in \mathcal{F}_T

ρ - Position vector from Target Body CM to Spacecraft CM, resolved in \mathcal{F}_I

A - 3×3 Spacecraft attitude as direction-cosine matrix

T - 3×3 Target Body attitude as direction-cosine matrix

The inner products in (3.6) can be calculated as,

$$\underline{N} \cdot \underline{\rho} = N_i^T (T\rho) = N_i^T T\rho \quad (3.10)$$

$$\underline{N} \cdot \underline{c} = (AT^T N_i)^T c_i = N_i^T T A^T c_i \quad (3.11)$$

$$\underline{N} \cdot \underline{d} = (AT^T N_i)^T d_i = N_i^T T A^T d_i \quad (3.12)$$

where the inner product (3.10) has been computed in \mathcal{F}_T and the inner products (3.11) and (3.12) have been computed in $\mathcal{F}_{s/c}$. Substituting inner product expressions (3.10)-(3.12) into (3.6) gives the range associated with the i 'th beam as,

$$|r_i| = \frac{\kappa_i - N_i^T T\rho - N_i^T T A^T c_i}{N_i^T T A^T d_i} \quad (3.13)$$

$$= \frac{\kappa_i - N_i^T T A^T c_i}{\gamma_i} - \frac{N_i^T T\rho}{\gamma_i} \quad (3.14)$$

where $\gamma_i \triangleq N_i^T T A^T d_i$.

Define the noisy range measurement associated with the i 'th beam as,

$$y_{ri} = |r_i| + n_i \quad (3.15)$$

$$Cov[n_i] = \sigma_i^2 \quad (3.16)$$

where the noise n_i is assumed to be white and independent from beam to beam. Rearranging (3.15) gives $|r_i| = y_{ri} - n_i$ which can be substituted into (3.14) to give,

$$y_{ri} - n_i = \frac{\kappa_i - N_i^T T A^T c_i}{\gamma_i} - \frac{N_i^T T\rho}{\gamma_i} \quad (3.17)$$

Rearranging (3.17) gives,

$$y_{ri} + \frac{N_i^T T A^T c_i - \kappa_i}{\gamma_i} = -\frac{N_i^T T\rho}{\gamma_i} + n_i \quad (3.18)$$

With a change of notation, this becomes,

$$y_i = h_i^T \rho + n_i \quad (3.19)$$

where,

$$y_i \triangleq y_{ri} + \frac{N_i^T T A^T c_i - \kappa_i}{\gamma_i}; \quad h_i^T \triangleq -\frac{N_i^T T}{\gamma_i} \quad (3.20)$$

Equation (3.20) is now noise-normalized to become,

$$\frac{y_i}{\sigma_i} = \frac{h_i^T}{\sigma_i} \rho + \frac{n_i}{\sigma_i} \quad (3.21)$$

or equivalently,

$$\tilde{y}_i = \tilde{h}_i^T \rho + \tilde{n}_i \quad (3.22)$$

where,

$$\tilde{y}_i \triangleq \frac{y_i}{\sigma_i}; \quad \tilde{h}_i^T \triangleq \frac{h_i^T}{\sigma_i}; \quad Cov[\tilde{n}_i] = 1 \quad (3.23)$$

Consider m beams, $i = 1, \dots, m$ associated with a particular RMT update. Stacking the normalized measurement (3.23) for each beam gives the stacked measurement equation,

$$Y_{stack} = H_{stack} \rho + n_{stack} \quad (3.24)$$

where,

$$Y_{stack} = \begin{bmatrix} \tilde{y}_1 \\ \vdots \\ \tilde{y}_m \end{bmatrix}; \quad H_{stack} = \begin{bmatrix} \tilde{h}_1^T \\ \vdots \\ \tilde{h}_m^T \end{bmatrix} \quad (3.25)$$

$$n_{stack} = \begin{bmatrix} \tilde{n}_1 \\ \vdots \\ \tilde{n}_m \end{bmatrix}; \quad Cov[n_{stack}] = I \quad (3.26)$$

For $m \leq 3$ equation (3.24) will be applied directly as the measurement update to the Kalman filter. This will require the in-flight inversion of at most a 3×3 matrix. For $m \geq 4$ a pre-processing step based on QR factorization will be applied.

The pre-processing step uses a QR factorization to improve numerical robustness, and also to ensure that only a 3×3 matrix needs to be inverted by the Kalman filter, even if there are 4 or more beams. Specifically, a QR decomposition of H_{stack} is taken of the form [9],

$$H_{stack} = QR = [Q_1, Q_2] \begin{bmatrix} R_{11} \\ 0 \end{bmatrix} = Q_1 R_{11} \quad (3.27)$$

where $R_{11} \in R^{3 \times 3}$. Multiplying (3.24) on the left by Q^T and using (3.27) gives the equivalent measurement equation,

$$Q^T Y_{stack} = \begin{bmatrix} R_{11} \\ 0 \end{bmatrix} \rho + Q^T n_{stack} \quad (3.28)$$

A key observation is that all but the top 3 equations of (3.28) are pure noise and can be removed from consideration. Keeping only the top 3 equations of (3.28) gives,

$$y_3 = R_{11} \rho + n_3 \quad (3.29)$$

where,

$$y_3 = Q_1^T Y_{stack}; \quad n_3 = Q_1^T n_{stack} \quad (3.30)$$

$$R_3 = Cov[n_3] = I \quad (3.31)$$

The algorithm checks the size of the diagonal elements of the rows of R_{11} (an upper triangular matrix) to see whether 1, 2, or 3 of the measurements in (3.29) should be applied for KF updating. The measurements can then be applied as scalar updates, or in a single update (requiring the KF to invert at most a 3×3 matrix).

At this point, the measurement equation (3.29) is in the form of a linear function of the relative position ρ , and can be directly incorporated into any Kalman filter mechanization that contains ρ as part of its state vector (cf., [1][2]). A simple small body state estimator is considered later in this paper where the state is defined as,

$$x = \begin{bmatrix} \rho \\ \dot{\rho} \end{bmatrix} \quad (3.32)$$

and $\dot{\rho}$ denotes the relative velocity with respect to an inertial frame. Using the full state definition (3.32) one can write ρ as,

$$\rho = [I, 0]x \quad (3.33)$$

Substituting (3.33) into (3.29) gives the final measurement equation of the form,

$$y_{RMT} = H_{RMT}x + n_{RMT} \quad (3.34)$$

where,

$$H_{RMT} = [R_{11}, 0] \quad (3.35)$$

It is worth noting that we have postponed this last step to restrict the number of columns of H_{stack} to only 3. This minimizes the computational load associated with the QR factorization of H_{stack} in (3.27), which is proportional to the number of its columns squared. Specifically, the QR factorization of H_{stack} requires approximately $\frac{1}{2}mn^2$ flops (cf., [14]), where m is the number of beams, and $n = 3$ is the number of columns.

The measurement equation (3.34) for facet-based altimetry has been used with the Kalman filter developed in [1][2] for studying space exploration of small bodies.

4 VELOCITY MEASUREMENT TABLE (VMT)

The Velocimeter Table (VMT) is a table of measured inertial velocities along known Doppler radar beam directions. The format of the VMT is shown in Table 4.2, where each row of the VMT corresponds to a velocity measurement along a different beam direction. There are m rows corresponding to at most m possible beams. While the actual number of beams is not limited, 3 or 4 beams are typical. The first column is the row index, and the second column is a number from 0 to 1 representing the confidence in the measurement. For the present, these confidences are taken as either 0 or 1, indicating a complete rejection or acceptance of the measurement, respectively. The quantity y corresponds to the Doppler velocity measurement from the i 'th beam, and σ is its associated 1-sigma error value. Currently, noises on each beam are assumed independent. The quantity f is the location of the beam's intercept point on the surface of the target body, and $Cov[f - f_{true}]$ is its associated covariance. Typically, the intersection point f is not known exactly, and must be estimated using a shape model, and the current state estimate. The quantity c represents the offset from the spacecraft CM to the sensor origin, and d represents the unit vector direction of the beam.

Velocimeter Table (VMT)

#	Conf	$y =$ $d^T \dot{r}$	σ	$f^T =$ $[f_x, f_y, f_z]$	$Cov[f - f_{true}] =$ $[P_{xx}, P_{xy}, P_{xz} P_{yy}, P_{yz} P_{zz}]$	d^T	c^T
1							
2							
\vdots							

Table 4.2: Velocimeter Table (VMT) specifying velocity along known directions

Let all vectors with under-arrows (e.g., \underline{x}), be coordinate free. The beam index i will also be dropped for the time being, and we will consider a generic beam. Then from geometry,

$$\underline{r} = -\underline{\rho} - \underline{c} + \underline{f} \quad (4.1)$$

Given a coordinate-free vector \underline{x} , let its inertial derivative be denoted by $\dot{\underline{x}}$, its derivative with respect to the spacecraft body frame be denoted by $\overset{o}{\dot{\underline{x}}}$, and its derivative with respect to the rotating target body be denoted by $\overset{t}{\dot{\underline{x}}}$. Then we have the following relationships,

$$\dot{\underline{c}} = \overset{o}{\dot{\underline{c}}} + \underline{\omega}_{sc} \times \underline{c} = \underline{\omega}_{sc} \times \underline{c} \quad (4.2)$$

$$\dot{\underline{f}} = \overset{t}{\dot{\underline{f}}} + \underline{\omega}_T \times \underline{f} = \underline{\omega}_T \times \underline{f} \quad (4.3)$$

where we have used the fact that \underline{c} is fixed in the spacecraft body (i.e., $\overset{o}{\dot{\underline{c}}} = 0$), and f is fixed in the target body (i.e., $\overset{t}{\dot{\underline{f}}} = 0$).

Taking the inertial derivative of (4.1) and substituting (4.2)(4.3) yields,

$$\underline{\dot{r}} = -\underline{\dot{\rho}} - \underline{\dot{c}} + \underline{\dot{f}} \quad (4.4)$$

$$= -\underline{\dot{\rho}} - \underline{\omega}_{sc} \times \underline{c} + \underline{\omega}_T \times \underline{f} \quad (4.5)$$

The physical Doppler measurement z_v is precisely the component of the inertial velocity vector $\underline{\dot{r}}$ projected along a given beam direction \underline{d} . This is obtained as the dot product of \underline{d} with $\underline{\dot{r}}$ obtained from (4.5) as follows,

$$z_v = \underline{d} \cdot \underline{\dot{r}} \quad (4.6)$$

$$= -\underline{d} \cdot \underline{\dot{\rho}} - \underline{d} \cdot (\underline{\omega}_{sc} \times \underline{c}) + \underline{d} \cdot (\underline{\omega}_T \times \underline{f}) \quad (4.7)$$

This is the desired coordinate-free expression for the Doppler observable.

Now the variables $z_{vi}, c_i, d_i, f_i, r_i, \dot{r}_i$ are specialized to be associated with the i 'th beam, and the following choices are made for the various coordinate frames,

$$c_i, d_i, \omega_{sc} \in \text{S/C body frame } \mathcal{F}_{sc} \quad (4.8)$$

$$r_i, \rho, \dot{r}_i, \dot{\rho} \in \text{Inertial frame } \mathcal{F}_I \quad (4.9)$$

$$f_i, \omega_T \in \text{Target body frame } \mathcal{F}_T \quad (4.10)$$

where,

r_i, \dot{r}_i - Position and velocity vectors from i 'th Radar beam origin to its intersection point on Target body, resolved in Inertial \mathcal{F}_I

f_i - Position vector from Target body CM to i 'th intersection point on Target body, resolved in \mathcal{F}_T

c_i - Position vector from Spacecraft CM to Radar beam origin, resolved in \mathcal{F}_{sc}

d_i - Unit vector direction of i 'th Radar beam, resolved in \mathcal{F}_{sc}

A - 3×3 Spacecraft attitude as DCOS matrix, $A = A(q_{sc})$

T - 3×3 Target attitude as DCOS matrix, $T = T(q_T)$

Using this notation, equation (4.7) can be specialized to give,

$$y_{vi} = z_{vi} + n_i \quad (4.11)$$

$$= -d_i^T A \dot{\rho} - d_i^T \omega_{sc}^\times c_i + d_i^T A T^T \omega_T^\times f_i + n_i \quad (4.12)$$

where y_{vi} is the velocity measurement associated with the i 'th Doppler beam, and $n_i \sim N(0, \sigma_i^2)$ has been included to denote additive measurement noise. Equation (4.12) is the desired expression for the Doppler measurement y_{vi} associated with the i 'th radar beam.

In order to best incorporate (4.12) into the state estimator update, a pseudo-measurement y_i is defined as,

$$y_i = y_{vi} + d_i^T \omega_{sc}^\times c_i - d_i^T A T^T \omega_T^\times f_i \quad (4.13)$$

Then, by this construction,

$$y_i = -d_i^T A \dot{\rho} + n_i \quad (4.14)$$

which has the desired form of being linear in the state $\dot{\rho}$.

The measurement (4.14) is noise-normalized as,

$$\tilde{y}_i = y_i / \sigma_i = -\frac{d_i^T A \dot{\rho}}{\sigma_i} + \frac{n_i}{\sigma_i} \quad (4.15)$$

$$= \tilde{h}_i^T \dot{\rho} + \tilde{n}_i \quad (4.16)$$

where,

$$\tilde{h}_i = -\frac{A d_i}{\sigma_i}; \quad Cov[\tilde{n}_i] = 1 \quad (4.17)$$

Consider m beams, $i = 1, \dots, m$ associated with a particular VMT update. Stacking the normalized measurement (4.16) for each beam gives the stacked measurement equation,

$$Y_{stack} = H_{stack} \dot{\rho} + n_{stack} \quad (4.18)$$

where,

$$Y_{stack} = \begin{bmatrix} \tilde{y}_1 \\ \vdots \\ \tilde{y}_m \end{bmatrix}; \quad H_{stack} = \begin{bmatrix} \tilde{h}_1^T \\ \vdots \\ \tilde{h}_m^T \end{bmatrix} \quad (4.19)$$

$$n_{stack} = \begin{bmatrix} \tilde{n}_1 \\ \vdots \\ \tilde{n}_m \end{bmatrix}; \quad Cov[n_{stack}] = I \quad (4.20)$$

For $m \leq 3$ equation (4.18) will be applied directly as a measurement update to the Kalman filter. This will require the in-flight inversion of at most a 3×3 matrix. For $m \geq 4$ a pre-processing step based on QR factorization will be applied.

The pre-processing step uses a QR factorization to improve numerical robustness, and also to ensure that only a 3×3 matrix needs to be inverted by the Kalman filter, even if there are 4 or more beams. Specifically, a QR decomposition of H_{stack} is taken of the form,

$$H_{stack} = QR = [Q_1, Q_2] \begin{bmatrix} R_{11} \\ 0 \end{bmatrix} = Q_1 R_{11} \quad (4.21)$$

where $R_{11} \in R^{3 \times 3}$. Multiplying (4.18) on the left by Q^T and using (4.21) gives the equivalent measurement equation,

$$Q^T Y_{stack} = \begin{bmatrix} R_{11} \\ 0 \end{bmatrix} \dot{\rho} + Q^T n_{stack} \quad (4.22)$$

A key observation is that all but the top 3 equations of (4.22) are pure noise and can be removed from consideration. Keeping only the top 3 equations of (4.22) gives,

$$y_3 = R_{11} \dot{\rho} + n_3 \quad (4.23)$$

where,

$$y_3 = Q_1^T Y_{stack}; \quad n_3 = Q_1^T n_{stack} \quad (4.24)$$

$$R_3 = Cov[n_3] = I \quad (4.25)$$

As with the RMT update, the algorithm checks the size of the diagonal elements of the rows of R_{11} (an upper triangular matrix) to see whether 1, 2, or 3 of the measurements in (4.23) should be applied for KF updating.

Given a full state vector x of the form,

$$x = \begin{bmatrix} \rho \\ \dot{\rho} \end{bmatrix} \quad (4.26)$$

one can write $\dot{\rho}$ as,

$$\dot{\rho} = [0, I]x \quad (4.27)$$

Substituting (4.27) into (4.23) gives the final measurement equation of the form,

$$y_{VMT} = H_{VMT}x + n_{VMT} \quad (4.28)$$

where,

$$H_{VMT} = [R_{11}, I] \quad (4.29)$$

As with the RMT update, we have intentionally postponed this last step to restrict the number of columns of H_{stack} to only 3.

REMARK 4.1 [Single Frame Estimate for VMT] A single-frame estimate of $\dot{\rho}$ can be defined from (4.23) by inverting the matrix R_{11} to give,

$$\hat{\dot{\rho}} = R_{11}^{-1} y_3 \quad (4.30)$$

Physically, R_{11} is invertible if 3 or more radar beams listed in the VMT are non-coincident. Mathematically, R_{11} is upper triangular, so invertibility can be tested in-flight by considering only its diagonal entries. Assuming R_{11}^{-1} exists, the estimate (4.30) has covariance,

$$Cov[\hat{\dot{\rho}}] = E[(\dot{\rho} - \hat{\dot{\rho}})(\dot{\rho} - \hat{\dot{\rho}})^T] = R_{11}^{-1} R_{11}^{-T} \quad (4.31)$$

Note that this covariance is useful because it indicates how much information is contained solely in the current VMT. Single frame estimates are important for debugging purposes, performance monitoring, and real-time fault diagnosis and recovery. ■

5 ESTIMATION FRAMEWORK

5.1 Dynamics

A simple estimation framework is introduced for the purpose of demonstrating use of the measurement updates developed earlier. The second-order dynamics of a spacecraft around a target body can be written as,

$$\ddot{\rho} = u + \tilde{w} \quad (5.1)$$

where u is exogenous,

$$u = \mathbf{1}(t) \cdot a_m - a_T^o + g(r_T^o, \rho^o) \quad (5.2)$$

and \tilde{w} is random,

$$\tilde{w} = \mathbf{1}(t) \cdot w_a + w_{sc} - w_T + w_g \quad (5.3)$$

$$\tilde{Q} \triangleq \text{Cov}(\tilde{w}) = \mathbf{1}(t) \cdot Q_a + Q_b \quad (5.4)$$

$$Q_a = \text{Cov}(w_a)$$

$$Q_b = \text{Cov}(w_{sc} - w_T + w_g) \quad (5.5)$$

where,

$$\mathbf{1}(t) \triangleq \begin{cases} 1 & \text{if a thruster is firing} \\ 0 & \text{Otherwise} \end{cases} \quad (5.6)$$

a_m - accelerometer measurement from the Inertial Measurement Unit (IMU) (m/s^2) with measurement error w_a

w_{sc} and w_T - unmodeled specific accelerations on the spacecraft and target body, respectively

a_T^o - nominal (known) specific acceleration of the Target Body

ρ^o and r_T^o - nominal values of the relative position ρ and target position r_T , respectively

$g(\cdot, \cdot)$ - gravity model used by the estimator

w_g - unmodeled gravity effects

Equation (5.1) can be put into matrix form as,

$$\dot{x} = Ax + \tilde{B}u + \tilde{\Gamma}\tilde{w} \quad (5.7)$$

where,

$$x = \begin{bmatrix} \rho \\ \dot{\rho} \end{bmatrix}; A = \begin{bmatrix} 0 & I \\ 0 & 0 \end{bmatrix}; \tilde{B} = \begin{bmatrix} 0 \\ I \end{bmatrix}; \tilde{\Gamma} = \begin{bmatrix} 0 \\ I \end{bmatrix} \quad (5.8)$$

$$\tilde{Q} \triangleq Cov(\tilde{w}) = I(t) \cdot Q_a + Q_b \quad (5.9)$$

As a last step, the state-space form (5.8) is discretized in time assuming that $u(t)$ is piecewise constant over T to give,

$$x_{k+1} = Fx_k + \bar{B}u_k + w_k \quad (5.10)$$

where,

$$F = e^{AT} = \begin{bmatrix} I & T \cdot I \\ 0 & I \end{bmatrix}; \quad \bar{B} = \begin{bmatrix} \frac{T^2}{2} \cdot I \\ T \cdot I \end{bmatrix} \quad (5.11)$$

$$Cov(w_k) \triangleq Q_k = \begin{bmatrix} \frac{T^3}{3} \tilde{Q} & \frac{T^2}{2} \tilde{Q} \\ \frac{T^2}{2} \tilde{Q} & T \cdot \tilde{Q} \end{bmatrix} \quad (5.12)$$

5.2 Kalman Filter Time Update

The Kalman filter time-update for the model (5.10) is given as,

$$\hat{x}_{k+1|k} = F\hat{x}_{k|k} + \bar{B}u_k \quad (5.13)$$

$$M_{k+1} = FP_kF^T + Q_k \quad (5.14)$$

5.3 Kalman Filter Measurement Update

Assume all relevant small-body measurements (e.g., RMT, VMT, etc.), are available in the form,

$$y_k = H_k x_k + n_k \quad (5.15)$$

$$Cov[n_k] = R_k \quad (5.16)$$

The Kalman filter measurement-update for (5.15)(5.16) is given as,

$$\begin{aligned} \hat{x}_{k|k} &= \hat{x}_{k|k-1} + K_k(y_k - H_k \hat{x}_{k|k-1}) \\ K_k &= M_k H_k^T \left((1 + \mathbf{uw}) H_k M_k H_k^T + R_k \right)^{-1} \end{aligned} \quad (5.17)$$

$$P_k = (I - K_k H_k) M_k (I - K_k H_k)^T + K_k R_k K_k^T \quad (5.18)$$

The option for using underweighting $\mathbf{uw} > 0$ is inherited from the NASA Apollo program, and intentionally slows adaptation in linearized estimators. Joseph's form (5.18) ensures covariances will be propagated correctly even when using underweighted (i.e., suboptimal) gains.

6 CASE STUDIES

A case study is presented to show the effective combination of using an altimeter measurement with a camera measurement. Intuitively, the altimeter measures vertical information while the camera measures horizontal information. Since camera measurements are in the form of angles, the altimeter further supplies essential scale information. Consequently, the two sensors work together in a synergistic fashion to cover all three dimensions of translational motion.

The main camera measurement type is that of bearing angles to known landmarks. A listing of such bearing angles with their associated landmark locations constitutes the landmark table (LMT) data type. The LMT data type has been treated elsewhere [1][2]. The simulations in this section assume that the LMT measurement is comprised of only single landmark which updates the filter at a rate of once per minute. The real-time throughput needed for this low-rate LMT measurement is not expected to stress current spacecraft computers. An accelerometer having a 20 micro-g bias is also integrated into the filter solution. The altimeter measurement is assumed to be single beam, with a random error of 2 percent of range.

The dimensions of the small body is $544 \times 303 \times 268$ (m), and has a facet model with 242 facets shown in Figure 6.1. The navigation filter assumes that attitude information is available from a separate attitude filter (e.g., driven by star-tracker and gyro measurements), so does not carry extra states for attitude. A random attitude error of 10 arcseconds is assumed in all simulations.

A simulated descent trajectory from 1.5 km to 10 meters altitude is shown in Figure 6.2. The coordinates as a function of time are given in Figure 6.3. The coordinates of all plotted variables are in a East-North-Up (ENU) landing frame whose origin is on the shape model surface, located directly below the desired terminal altitude point. Position estimation errors associated with using LMT measurements alone are shown in Figure 6.4. The benefit from adding the altimeter measurement is shown in Figure 6.5. Here it is seen that the altimeter causes position errors in all three axes to drop earlier in the descent, and to values that are significantly smaller in magnitude than without using the altimeter. These same two plots are shown zoomed after 1500 (s) in Figure 6.6 and Figure 6.7, respectively, to show this comparison in more detail.

Velocity estimation errors associated with using LMT measurements alone are shown in Figure 6.8. The benefit from adding an altimeter measurement is shown in Figure 6.9. The altimeter causes velocity errors in all three axes to drop earlier in the descent, and to values that are significantly smaller in magnitude than without using the altimeter. These same two plots are shown zoomed after 1500 (s) in Figure 6.10 and Figure 6.11, respectively, to show this comparison in more detail.

The synergy between the altimeter and camera is evidenced by the fact that the position and velocity estimation errors drop significantly along all three axes, rather than just the

vertical channel. Due to space limitations, simulations of the VMT measurement type are not treated here, but can be found in [1].

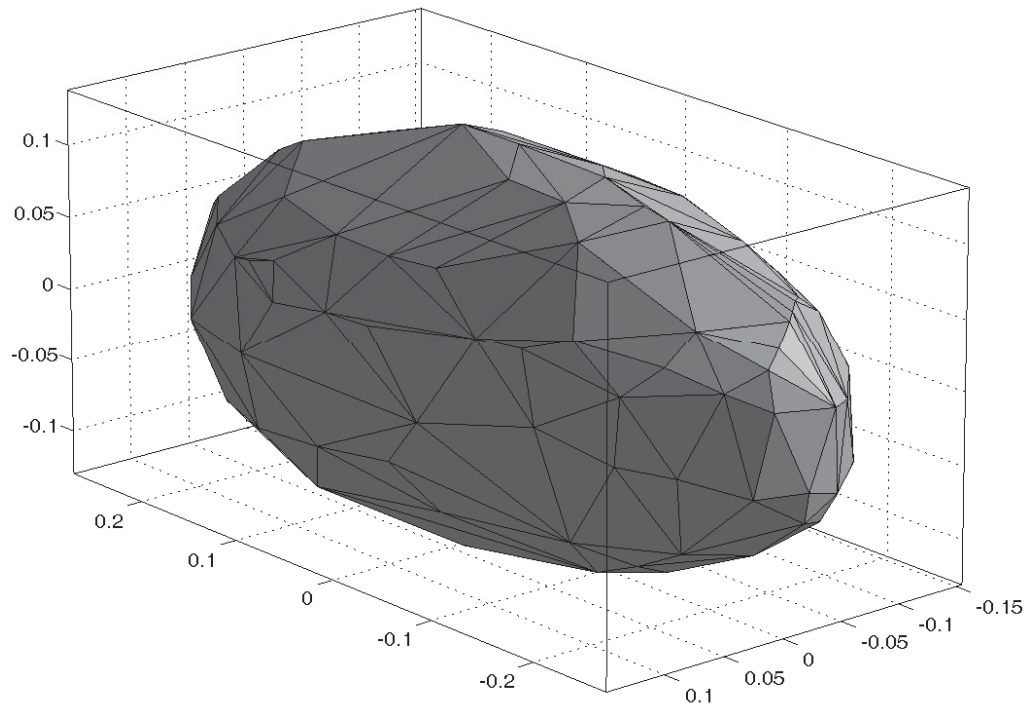


Figure 6.1: Shape model with 242 facets used for small body altimetry simulation study (km).

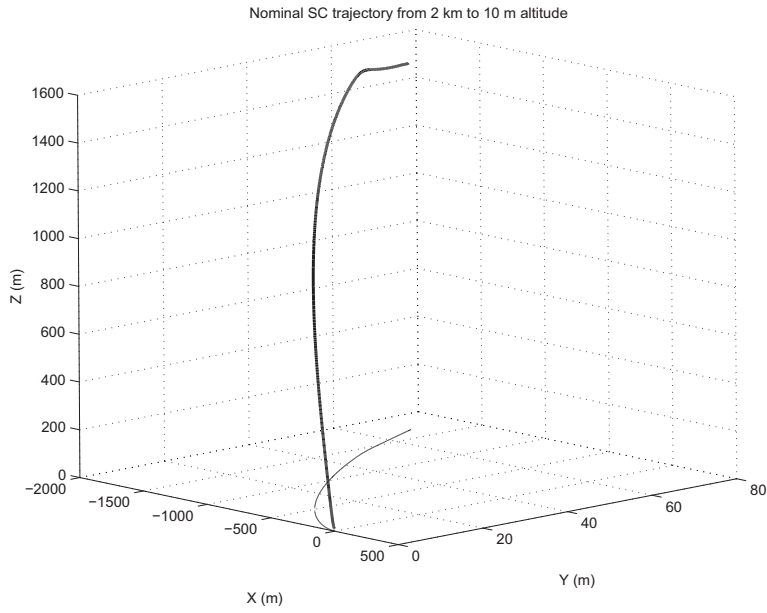


Figure 6.2: 3D plot of spacecraft trajectory including groundtrack in x-y plane.

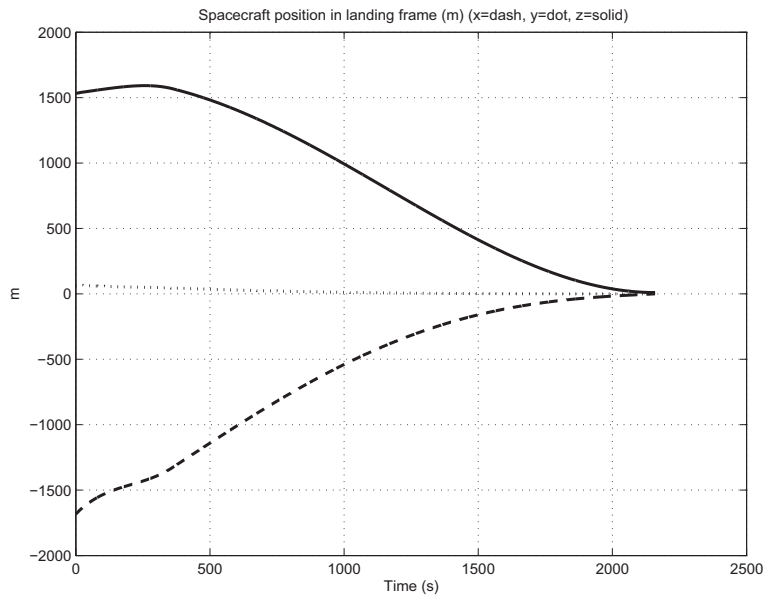


Figure 6.3: Coordinates of spacecraft trajectory ((x=dash, y=dot, z=solid)).

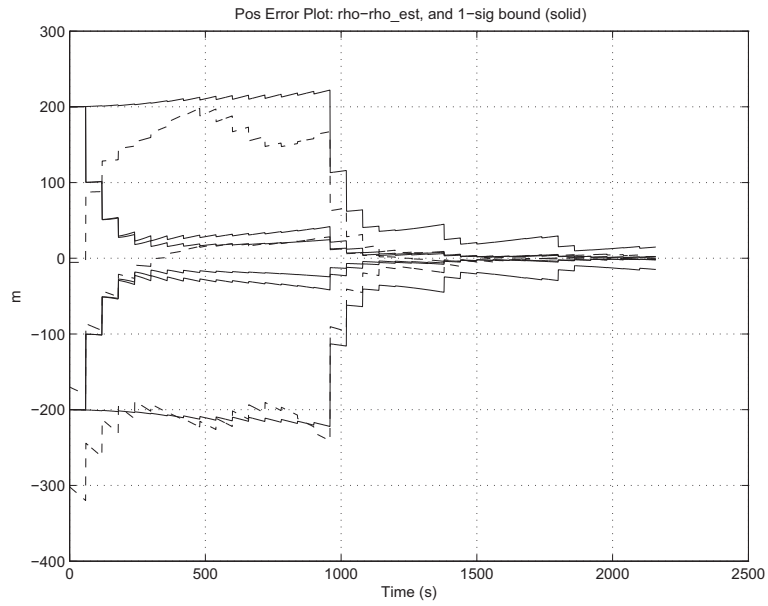


Figure 6.4: LMT-only case: Position error

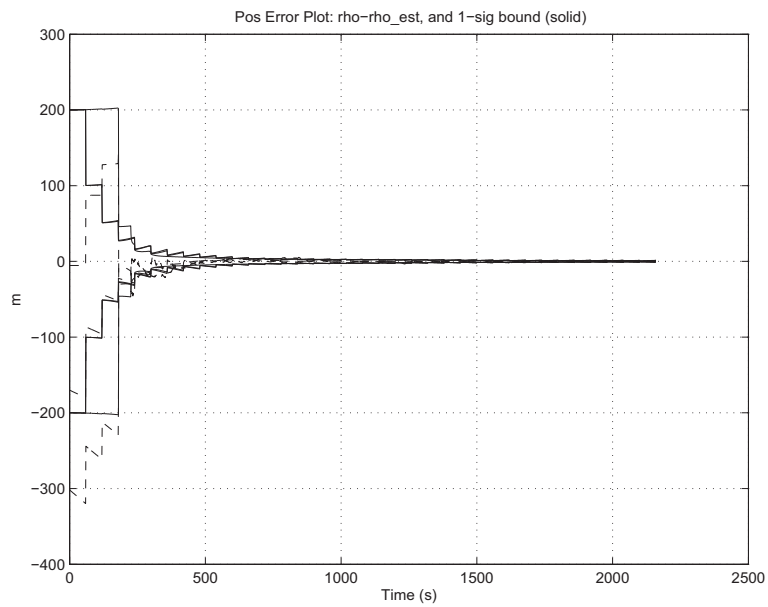


Figure 6.5: LMT+RMT case: Position error.

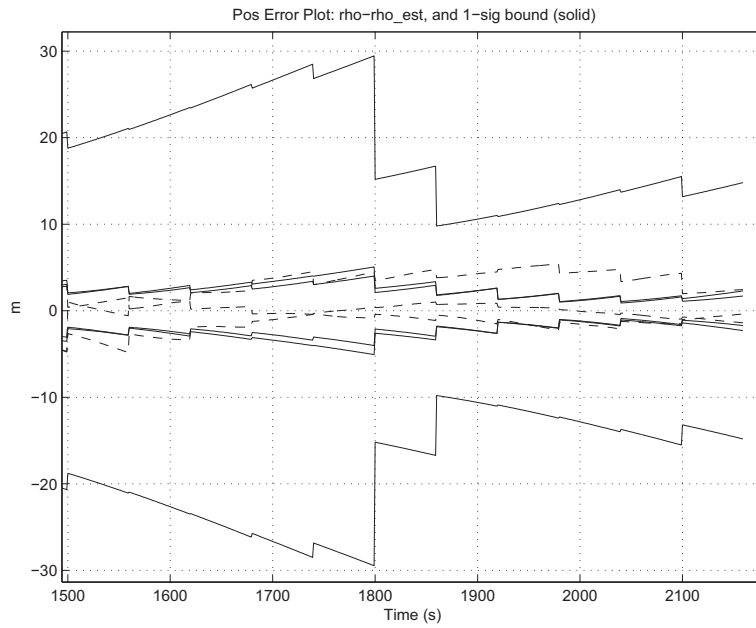


Figure 6.6: LMT-only case: Position error - zoomed.

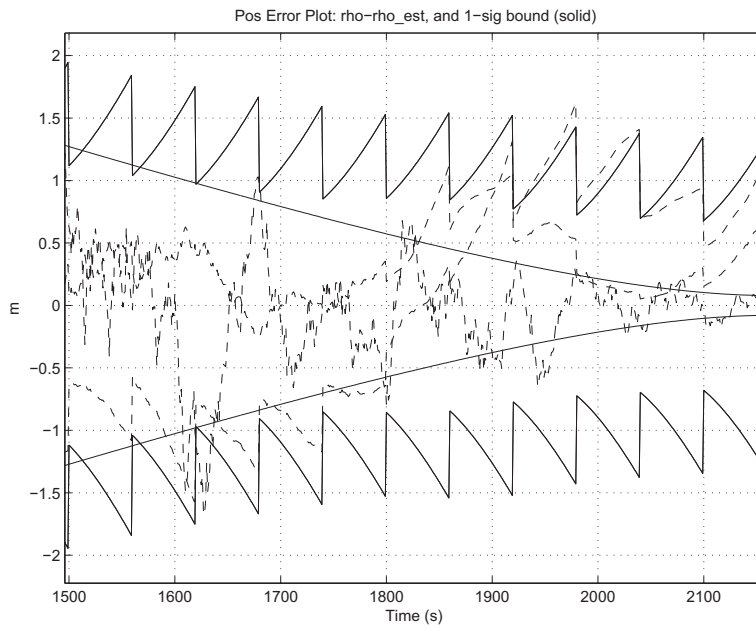


Figure 6.7: LMT+RMT case: Position error - zoomed.

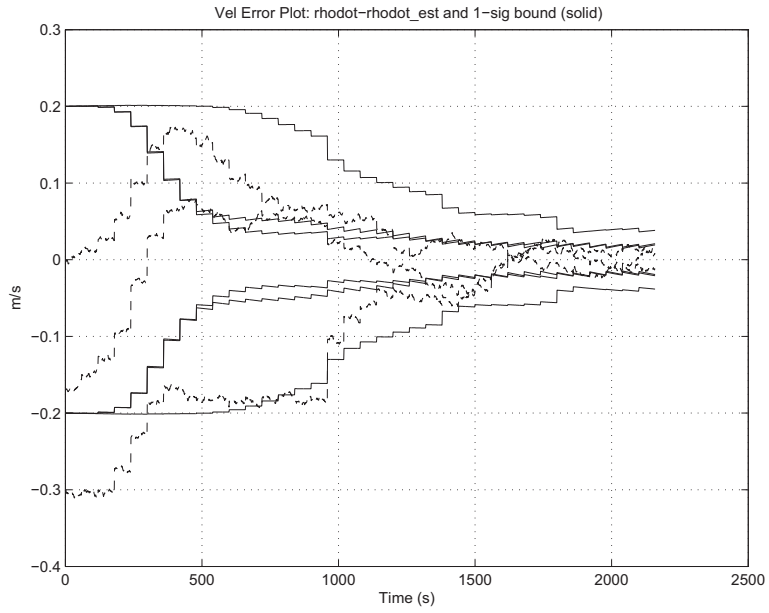


Figure 6.8: LMT-only case: Velocity error.

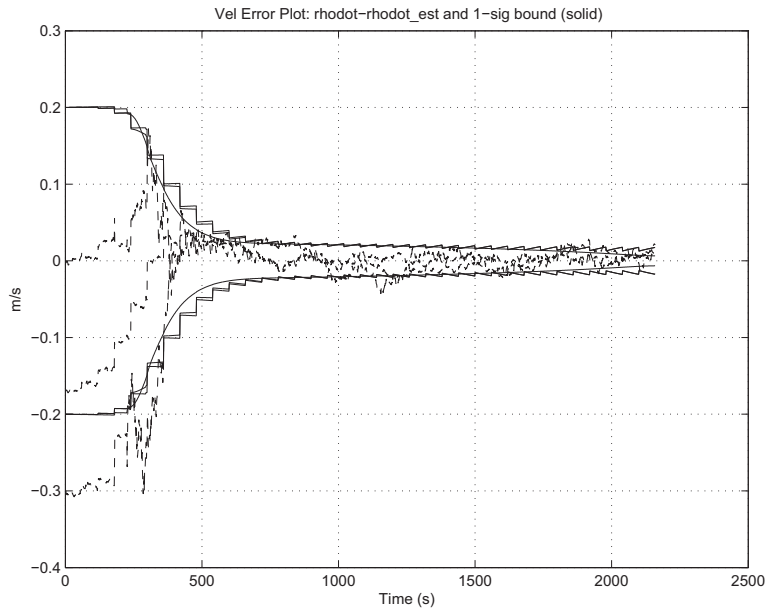


Figure 6.9: LMT+RMT case: Velocity error.

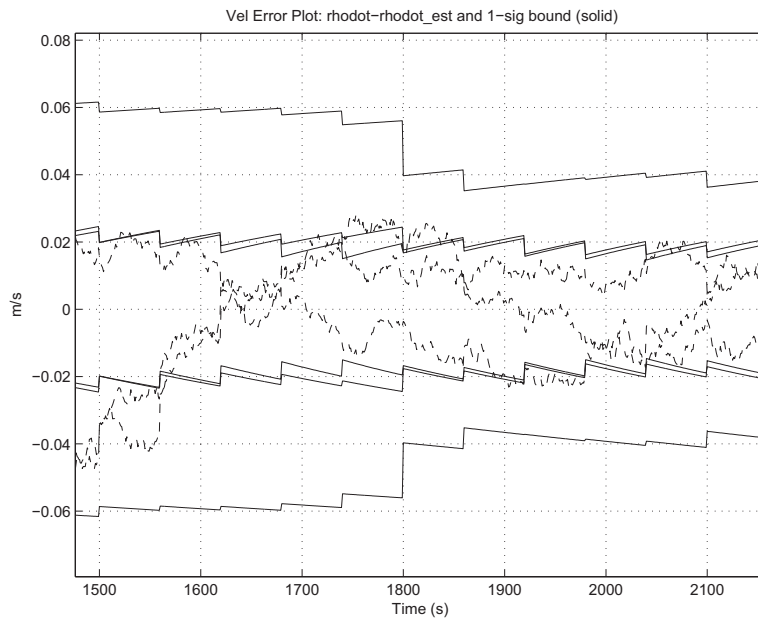


Figure 6.10: LMT-only case: Velocity error - zoomed.

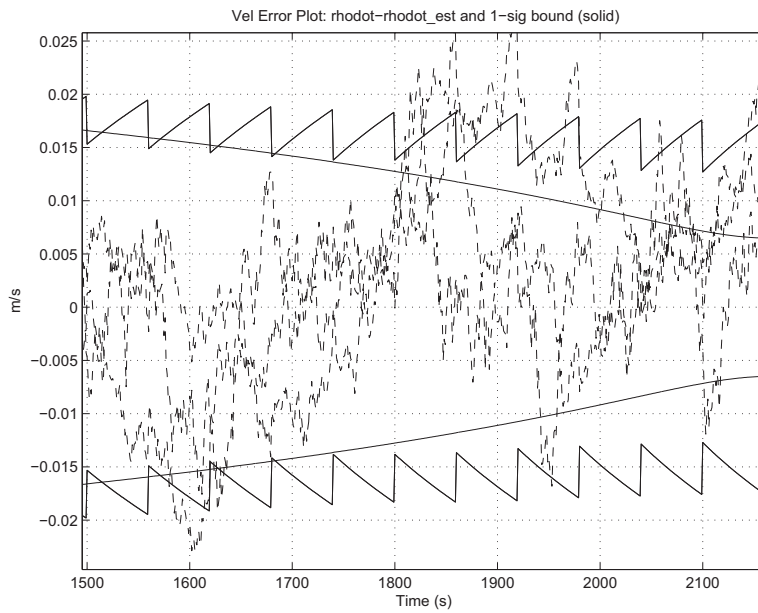


Figure 6.11: LMT+RMT case: Velocity error - zoomed.

7 DISCUSSION

The altimeter and Doppler velocimeter measurement updates make use of the faceted shape model in slightly different ways. While both require the calculation of the beam intersection point of each sensor beam with the target body shape model (giving the intersection location vector f), the RMT update requires knowing only the associated facet surface normal N and facet constant κ , rather than f . In other words, the altimeter update requires knowing which facet was intersected rather than the exact point of intersection. This should be contrasted with the VMT update that requires knowledge of the intersection location f for each beam. Intuitively, since the target body is rotating, the inertial velocity of the intersection point (seen by the Doppler measurement), depends on its location f on the target body.

The current paper deals with a Doppler type velocity measurement. A velocity measurement based on a time-of-flight type sensor is fundamentally different, and requires different information from the facet model. More details can be found in [6].

Because the beam intersection points must be calculated in real time, the number of facets retained in the facet model drives the complexity of the on-board computation. The case study uses a shape model with 242 facets, and assumes an altimeter update every 1 second. It is expected that these values can be accommodated by current spacecraft computers.

Generally speaking, the density of facets should be chosen commensurate with the roughness of the terrain. However, a high density of facets is not required when the spacecraft is far from the target body. For this reason, it may be desirable to carry different on-board facet models for different phases of the mission. For close proximity operations, the density of facets can be increased in areas where the altimeter is expected to be used. Aside from altimetry, the same facet models might be useful for calculating gravitational forces (assuming constant material density).

If estimation error is large with respect to the physical size of the facets, it is possible that the measurement updates will be made using facet information from the wrong facet. This effect has been simulated, and found to be small as long as the surface normals do not change grossly in the vicinity of the beam. In this case, converging estimates eventually locate the estimated beam on the correct facet. When terrain is rough, however, some care must be taken to initialize the estimator with errors smaller than the average local facet size. The initial convergence period can be robustified to some extent by using information obtained by averaging neighboring facets. More work remains to quantify benefits from this approach.

ACKNOWLEDGEMENTS

This research was performed at the Jet Propulsion Laboratory, California Institute of Technology, under contract with the National Aeronautics and Space Administration, and funded through the internal Research and Technology Development program.

8 CONCLUSIONS

Methods are developed to systematically incorporate a multibeam altimeter and Doppler velocimeter measurement into an on-board spacecraft state estimator by making use of information from a faceted shape model representation of the target body surface. The faceted shape model representation is very general and does not place any restriction on the surface complexity. This allows the estimation method to be applicable to a broad class of irregularly shaped target bodies such as asteroids and comets.

References

- [1] D.S. Bayard and P.B. Brugarolas, *Small Body GN&C Research Report: State Estimator with Capability Upgrade*. Internal Document, JPL D-32951, September 23, 2005.
- [2] D.S. Bayard and P.B. Brugarolas, "An Estimation Algorithm for Vision-Based Exploration of Small Bodies in Space," Proc. 2005 American Control Conference, pp. 4589-4595, Portland Oregon, June 8-10, 2005.
- [3] D.S. Bayard and P.B. Brugarolas, *Small Body GN&C Research Report: State Estimator Multibeam Altimeter Measurement Update Using Faceted Shape Model of Landing Surface*. Internal Document, JPL D-36205, September 22, 2006.
- [4] S. Bhaskaran, J.E. Riedel, S.P. Synnott, "Autonomous Nucleus Tracking for Comet/Asteroid Encounters: The STARDUST Example," IEEE Aerospace Conference Proceedings, Vol 2, pp. 353-365, March 21-28, 1998.
- [5] S. Bhaskaran, J.E. Riedel, B.M. Kennedy, T.C. Wang, "Navigation of the Deep Space 1 Spacecraft at Borrelly," Paper AIAA 2002-4815, AIAA/AAS Astrodynamics Specialists Conference, Monterey, California, August 5-8, 2002.
- [6] S.B. Broschart, *Small Body GN&C Research Report: Geometric Formulation of Altimeter and Time-of-Flight Velocimeter Measurements*. Internal Document, JPL D-32851, August 26, 2005.
- [7] S.B. Broschart, *Small Body GN&C Research Report: Subroutines for Faceted Shape Model Computations: Ray Intersection Algorithm (SB1) and Mass Property Calculations (SB2)*. Internal Document, JPL D-32824, August 26, 2005.
- [8] A. Gelb (Ed.), *Applied Optimal Estimation*. The MIT Press, Cambridge, Massachusetts, 1984.
- [9] G.H. Golub and C.F. Van Loan, *Matrix Computations*. The John Hopkins University Press, Baltimore, Maryland, 1983.

- [10] J. de Lafontaine, "Autonomous Spacecraft Navigation and Control for Comet Landing," *J. Guidance, Control and Dynamics*, Vol. 15, No. 3, pp. 561-576, May-June 1992.
- [11] D.G. Kubitschek, "Impactor Spacecraft Targeting for the Deep Impact Mission to Comet Tempel 1," Paper AAS 03-615, AAS/AIAA Astrodynamics Specialists Conference, Big Sky Resort, Big Sky, Montana, August 3-7, 2003.
- [12] T. Kubota, T. Hashimoto, J. Kawaguchi, M. Uo, K. Shirakawa, "Guidance and navigation of the Hayabusa spacecraft for asteroid exploration and sample return mission," SICE-ICASE, Busan, Korea, pp. 2793-2796, October 2006.
- [13] W.M. Owen, T.C. Wang, "NEAR Optical Navigation at Eros," Paper AAS 01-376, AAS/AIAA Astrodynamics Specialists Conference, Quebec City, Quebec, Canada, July 30-August 2, 2001.
- [14] L.N. Trefethen and D. Bau, *Numerical Linear Algebra*, Society for Industrial and Applied Mathematics, Philadelphia, PA, 1977.
- [15] R.C. Wrede, *Introduction to Vector and Tensor Analysis*. Dover Publications, New York, 1972.